Atomic level mechanisms of graphene healing by methane-based plasma radicals

Atomic level mechanisms of graphene healing by methane-based plasma radicals

U. Khalilov,[1,2,3,*] M. Yusupov,[3,4] G. B. Eshonqulov,[5]
E. C. Neyts,[2] and G. R. Berdiyorov[6]

[1] School of Engineering, New Uzbekistan University, Tashkent, 100007, Uzbekistan
[2] Research group PLASMANT, Department of Chemistry, University of Antwerp, Universiteitsplein 1, Antwerp, 2610, Belgium
[3] Laboratory of Thermal Physics of Multiphase Systems, Arifov Institute of Ion-Plasma and Laser Technologies, Academy of Sciences of Uzbekistan, Tashkent, 100125, Uzbekistan
[4] School of Engineering, Akfa University, Tashkent, 111221, Uzbekistan
[5] Department of Physics, National University of Uzbekistan, Tashkent, Uzbekistan
[6] Qatar Environment and Energy Research Institute, Hamad Bin Khalifa University, Doha, Qatar

* e-mail: umedjon.khalilov@uantwerpen.be

Using quantum-mechanical calculations we predict the possibility of healing vacancy defects in graphene from methane-based plasma particles CH_x (x=1-3). Enhanced pinning of these particles is obtained at the edges of vacancy defects. When the temperature rises, the carbon atom of the plasma particles substitutes for the missing carbon atom at the defects, restoring the graphene network to its perfect hexagonal structure. Plasma particles are also found to be effective catalysts for the healing of Stone-Wales defects. The details of the healing mechanism are studied for the considered plasma radicals using nudged elastic band calculations. The obtained results provide a better understanding of plasma-assisted healing mechanisms of defective graphene.

I. INTRODUCTION

Graphene is the most promising 2D material for practical applications in different fields, such as photonics and electronics [1, 2], due to its unique mechanical, chemical and physical properties [3, 4]. Synthesized graphene through chemical processing is usually not perfect, i.e., it contains several types of structural defects, such as grain boundaries, vacancies, dislocations, impurity atoms and defects associated with changes in carbon-hybridization [5–7]. It is well known that such defects greatly change the structural, electronic, optical and other measurable properties of graphene, since these properties are very sensitive even to small changes in the honeycomb arrangement of carbon atoms (see Refs. [8, 9] for reviews). They also affect the absorption process of both metallic and non-metallic atoms/molecules on graphene. For example, deposition of metals and metal oxides occur mostly at defected sites of graphene [10, 11]; the presence of defects inhibits the clustering of transition met- als [12], while enhancing the adsorption of some reagents (e.g., thiyl and hydroxyl radicals) on graphene by creating new active sites [13, 14].

Several methods have been proposed and experimentally demonstrated in the past for tailoring the hexagonal 2D structure of graphene. For example, using scanning transmission electron microscopy, Zan et al. showed the possibility of healing large number of vacancies on graphene sheet under room temperature electron bombardment [15]. Song et al. also used focused ion beams to study the self-healing processes in graphene [16]. Thermal annealing more than 1000 K can also be an effective tool in self-healing the defects in graphene membrane [17, 18] and the use of metal catalysts further increases the efficiency of such thermal healing processes [19]. The sources of the extra carbon atoms for such knitting can be the hydrocarbon impurities near the membrane or the carbon atoms can be injected directly to the defect area from external sources [20]. However, additional and unwanted defects, such as linear carbon chains, blister-like structures, as well as non-hexagonal ring structures (e.g., Stone-Wales) can be formed during high temperature annealing or due to high electron irradiation doses [15, 20, 21].

In this work, we conduct reactive molecular dynamics (MD) simulations supported by density functional theory (DFT) calculations to study the possibility of healing graphene with a single vacancy defect using methane plasma radicals, i.e., CH_x (x=1-3). Recent experiments show the significant effect of low-temperature plasma treatment on the chemical properties of carbon fibers such as wettability [22]. Electronic properties of carbon-based materials also affected by the plasma treatment [23]. Ref. [24] presents recent review on the effect plasma treatment on the surface functionalization and modification of carbon nanotubes. Profound effect

of carbon monoxide atmospheric plasma treatment on surface functionalization of nanoscale carbon materials is reported by Zaldivar et al. [25]. Experiments also show the potential of low-temperature plasma treatment of surface functionalization of graphene [26–29]. Despite such an extensive research, the mechanisms of interaction of plasma particles with the surface of carbon-based materials remain not fully understood. Our simulation results show that all plasma species are chemisorbed on defective site of graphene, where the adsorption properties strongly depend on the parameters of the plasma particles. The adsorption becomes significantly stronger near the edges of the defects. At certain temperatures, the plasma particles start diffusing on the graphene surface until they get pinned at the defects. With further increase in temperature, the carbon atom of the plasma particles substitutes the missing carbon atom in the graphene and restores the planar hexagonal lattice. The reaction coordinates are studied using the nudged elastic band (NEB) calculations. The plasma treatment is predicted to be also effective in healing the larger vacancy defects, as well as Stone-Wales defect [30], which is one of the important topological defects with very large restoration energy (~6 eV) (see Ref. [31] for review). These results show the possibility of healing vacancy defects in graphene and thereby restoring its pristine properties by methane-based plasma radicals.

II. MODEL SYSTEMS AND COMPUTATIONAL APPROACHES

Our model system consists of a graphene supercell containing 60 carbon atoms without and with a single vacancy and divacancy defects. These defects are created by removing a corresponding number of carbon atoms from the hexagonal structure of graphene. We have also considered a Stone-Wales defect in graphene created by the rotating carbon-carbon bond of two neighboring atoms by 90°. Periodic boundary conditions are used along the graphene basal plane. Hydrocarbon radicals CH_x (x=1-3) are adsorbed on the surfaces of both pristine and defected graphene, see insets in Fig. 1 (a) and (b), respectively. The defected systems are optimized first before the adsorption of the plasma particles. The considered systems are described using the reactive force field ReaxFF to account for bond formation and breaking during the simulations [32]. The connectivity in the system is calculated in every iteration step taking into account both polarization effects and non-bounded interactions (van der Waals and Coulomb) [32]. Since the required parameters are obtained from the first-principles calculations, ReaxFF is known to be an effective tool in describing the structural and thermal properties of graphene and other carbon-based low-dimensional materials [33-38]. For example, this force field has been used to study the adsorption properties of CH_3 plasma particle on

pristine graphene [39] to interpret the experimental results [40]. Moreover, the ReaxFF-MD simulations were employed to study the growth mechanisms of carbon nanotubes using plasma particles [41, 42].

The model systems in this study are first energy-optimized using both ReaxFF and DFT. The latter was performed for the validation of the force field parameters. DFT calculations are conducted within the generalized gradient approximation of Perdew-Burke-Ernzerhof (PBE) to describe the exchange-correlation energy [43]. Van der Waals interactions are taken into account using Grimme's empirical correction to PBE [44]. The Brillouin zone is integrated using 3×2×1 Monkhorst-Pack *k*-points [45]. All atoms are described using double-zeta-polarized basis sets. The convergence criterion for Hellman-Feynman forces was 0.01 eV/Å in the calculations.

The reaction coordinates and transition states are calculated using the climbing image NEB method [46] which is known to be an effective method of studying the dynamics of small organic molecules on complex surfaces [47, 48]. The image-dependent pair potential method with minimum image convention is used to construct the initial path for the NEB calculations. All the atoms are relaxed during the NEB simulations with the residual forces in finding the transition states to be less than 0.05 eV/Å. NEB calculations are conducted using DFT.

MD simulations are conducted using the ReaxFF force field. The temperature of the geometry-optimized structures is increased up to 2500 K at a rate of 5 K/ps using an isothermal isobaric (NPT) ensemble at 1 atm pressure with a Berendsen thermostat and barostat [51]. The damping constants for temperature and pressure are 100 fs and 500 fs, respectively. The time step is used to be 0.25 fs in all simulations. The simulations are conducted for 500 ps during which the system temperature is increased from 0 K to 2500 K. We have also conducted constant temperature calculations for 500 ps. All calculations are conducted using the computational package Atomistix toolkit [49, 50].

III. ADSORPTION PROPERTIES OF CH_x RADICALS ON GRAPHENE

We start with studying the adsorption properties of CH_x plasma radicals on pristine and defected graphene. Figure 1 shows the adsorption energies of methane (CH_4) molecule and its plasma species (CH_x, x=1-3) on both pristine and defected graphene, obtained by DFT (solid-black curves) and ReaxFF (open-red curves) calculations. As an example, we consider a graphene sheet with a single vacancy defect. The adsorption energies are calculated as

$$E_{ads} = E_{sys} - \left(E_{graph} + E_{CH_x}\right) \quad (1)$$

where E_{sys} is the total energy of the system (i.e., graphene + plasma particle), E_{graph} is the total energy of graphene and E_{CH_x} is the total energy of the plasma radical. Insets show the optimized structures of the plasma particles in both pristine (a) and defected (b) graphene.

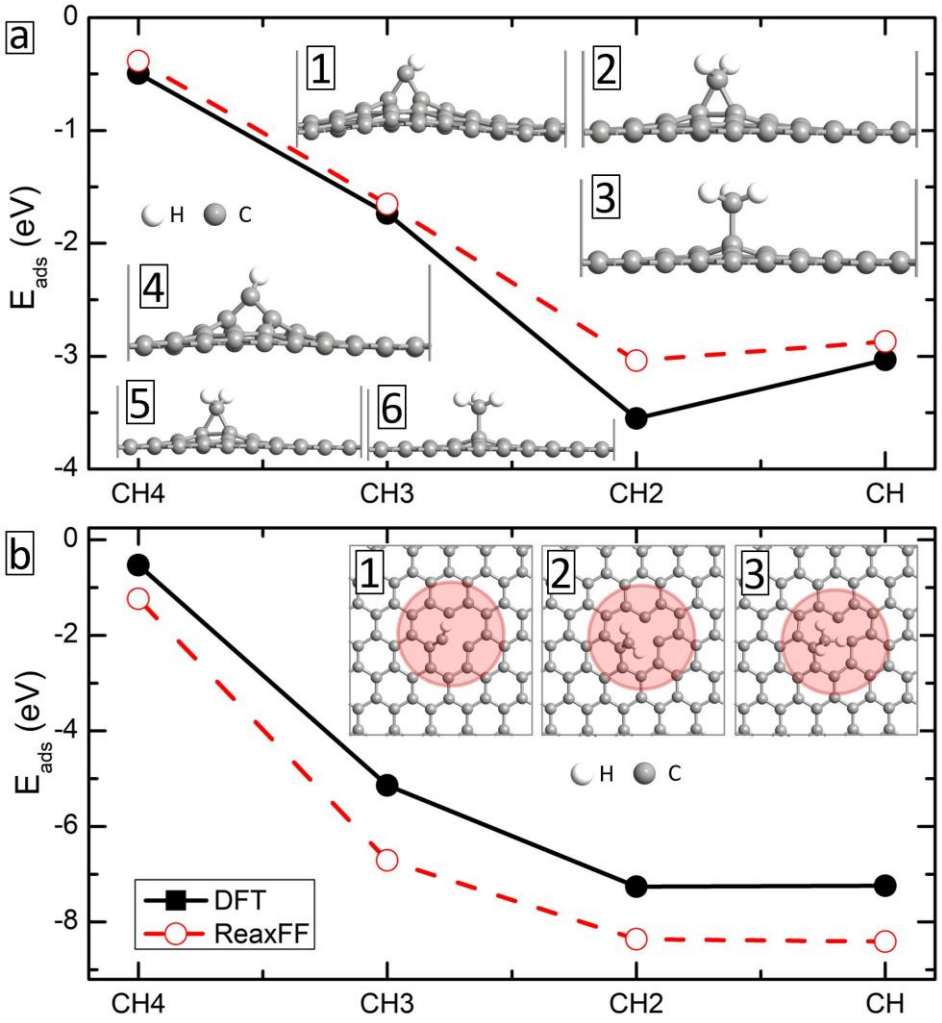

FIG. 1: Adsorption energies of methane (CH_4) molecule and its plasma radicals (CH_x (x=1-3)) on pristine (a) and single vacancy (b) graphene, calculated using DFT (solid-black circles) and ReaxFF force field (open-red circles) calculations. Defected areas in (b) are highlighted with a pale pink circle.

It is obvious that the smallest adsorption energy (i.e., weakest interaction) is obtained for CH_4 molecule in both samples. The molecule is physisorbed on the surface of graphene (not shown here). On the contrary, all other particles are chemisorbed with relatively high adsorption energies. In the case of pristine graphene, CH and CH_2 radicals prefer the bridge site adsorption (insets 1 and 2 in Fig. 1 (a)), whereas CH_3 radical makes top-side

adsorption (panel 3 in Fig. 1 (a)). Overall, the results indicate that the minimum adsorption energy (i.e., the strongest adsorption) is obtained for CH_2 plasma particle. In addition, it is clear from Fig. 1 that ReaxFF approach gives similar trends in the adsorption energies for all species, despite a small underestimation in the energy values. As a result, the energetically favorable configurations are also quite similar to the results of DFT (see insets 4-6 in Fig. 1 (a)). In the case of defected graphene, the adsorption of all the considered particles becomes stronger compared to the prestine graphene, i.e., the adsorption energies become more than twice larger in magnitude (see Fig. 1 (b)). The adsorption site of all particles is found at the edge of the defect (see insets in Fig. 1 (b)). The adsorption energies decrease monotonically (i.e., interaction becomes stronger) with decreasing the hydrogen content of the plasma particles. ReaxFF shows a similar trend in the adsorption energy as compared to DFT.

To find the origin for the stronger adsorption of the plasma radicals on defected graphene, we have calculated the electron difference density defined as the difference between the self-consistent valence charge density and the superposition of atomic valence densities. Figure 2 shows the isosurface plots of the electron difference density for CH_2 (a, b) and CH_3 (c, d) radicals adsorbed on pristine (a, c) and defected (b, d) graphene. Stronger charge exchange between the plasma particles and defected graphene is clearly seen in this figure. Consequently, the distance between the carbon atom of the plasma particle and graphene reduces due to the presence of the vacancy defect. For example, in the case of the CH_2 particle, this distance decreases from 1.52 Å to 1.36 Å.

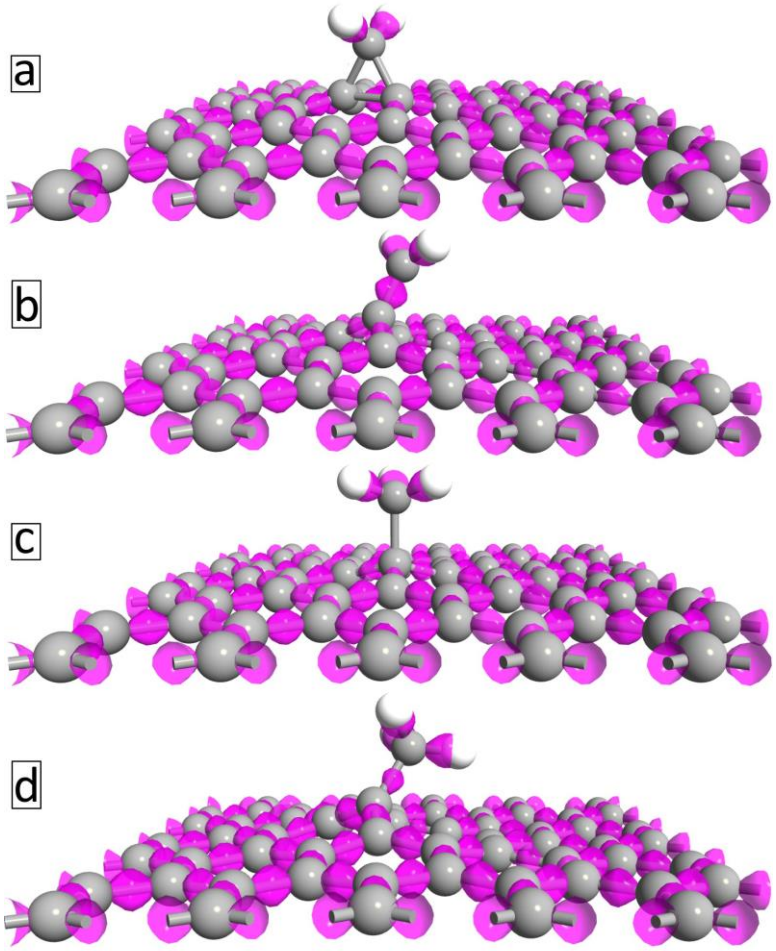

FIG. 2: Electron difference density plots for the adsorption of CH_2 (a, b) and CH_3 (c, d) on pristine (a, c) and defected (b, d) graphene. The isosurfaces are taken as ±0.28 e $Å^{-3}$.

IV. NUDGED ELASTIC BAND CALCULATIONS

In this section, we conduct NEB calculations to estimate the energies required for the expected healing of the graphene vacancy defects with plasma particles. Figure 3 shows the energy landscape during the healing of a single vacancy defect with CH_2 (a) and CH_3 (b) plasma radicals.

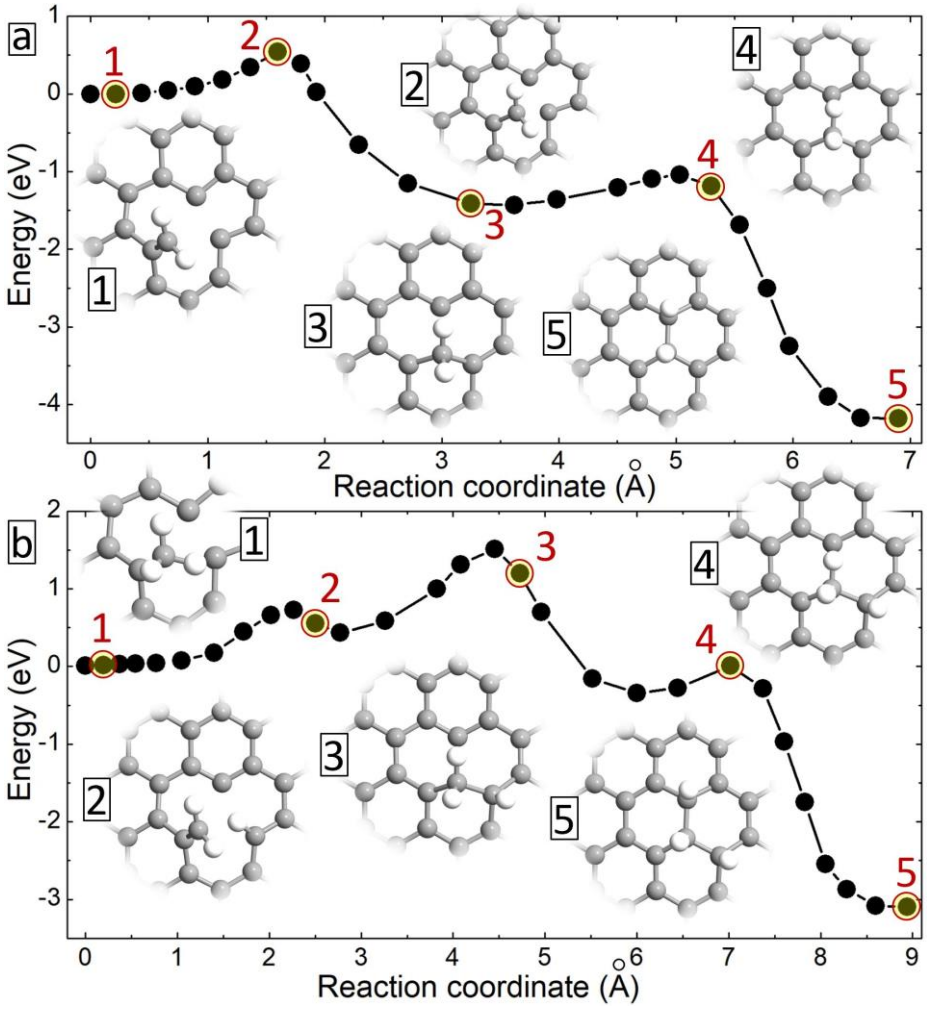

FIG. 3: The nudged elastic band energy profile for the healing process of a single vacancy defect in graphene with CH_2 (a) and CH_3 (b) plasma radicals. Insets show initial states (panels 1), final states (panels 5) and the intermediate states indicated on the energy curves.

In the first case, the NEB calculations yielded two saddle points separating one intermediate state. The first transition state is characterized by the formation of the covalent bond between the carbon atom of the molecule and the neighboring carbon atom of graphene (see point 2 and inset 2 in Fig. 3 (a)). The system transits to a local minimum with an energy gain of 1.43 eV (point 3 and inset 3 in Fig. 3 (a)). The barrier height for this transition is 0.54 eV. The system evolves further to the ground state configuration through another transition state characterized by the transfer of one of the hydrogen atoms of the molecule to the neighboring carbon atom (see inset 4 in Fig. 3 (a)). The barrier height for this reaction is 0.39 eV. The final state corresponds to pristine graphene with hydrogen atoms attached to some of the carbon atoms (see inset 5 in Fig. 3 (a)). Note that the minimum energy paths including the energy barrier for the healing of graphene are provided using only the initial and final states during NEB calculations.

Figure 3 (b) shows the potential energy profile during the healing of the vacancy defect by the

CH_3 particle. The initial state (panel 1 in Fig. 3 (b)) evolves to an intermediate state where one of the hydrogen atoms of CH_3 is transferred to a neighboring carbon atom with a dangling bond (panel 2 in Fig. 3 (b)). The calculated barrier for this transition is 0.72 eV. The next metastable state is characterized by the formation of the covalent bond between the carbon atom of the molecule and the graphene sheet (panel 3 in Fig. 3 (b)). The transition state energy is found to be 1.08 eV. The last transition state with an energy barrier of 0.33 eV corresponds to further deprotonation of the plasma particle (panel 4 in Fig. 3 (b)). The final state results in an energy gain of 3.1 eV and corresponds to a pristine graphene sheet (panel 5 in Fig. 3 (b)). Thus, the considered plasma particles can heal the vacancy defect in graphene by heating the system.

V. MOLECULAR DYNAMICS SIMULATIONS

In this section, we conduct ReaxFF MD calculations to study the healing processes of defected graphene by CH_x plasma radicals. As a reference, we start by considering the dynamics of the plasma particles on pristine graphene. Figure 4 shows the potential energy variations of pristine graphene as functions of reservoir temperature and time for the considered plasma particles. We do not obtain the desorption of CH and CH_2 particles during our 500 ps simulations (see insets in Fig. 4 (a) and (b)), despite their thermal-induced diffusions on the graphene (see supplemental online videos 1 and 2). On the other hand, the desorption of the CH_3 molecule takes place at high temperatures (see insets in Fig. 4 (c)) [39], resulting in a small drop and change in the slope of the potential energy curve. This plasma particle is also found to be mobile on graphene. No imperfections are obtained in the planar structure of graphene during the temperature increase.

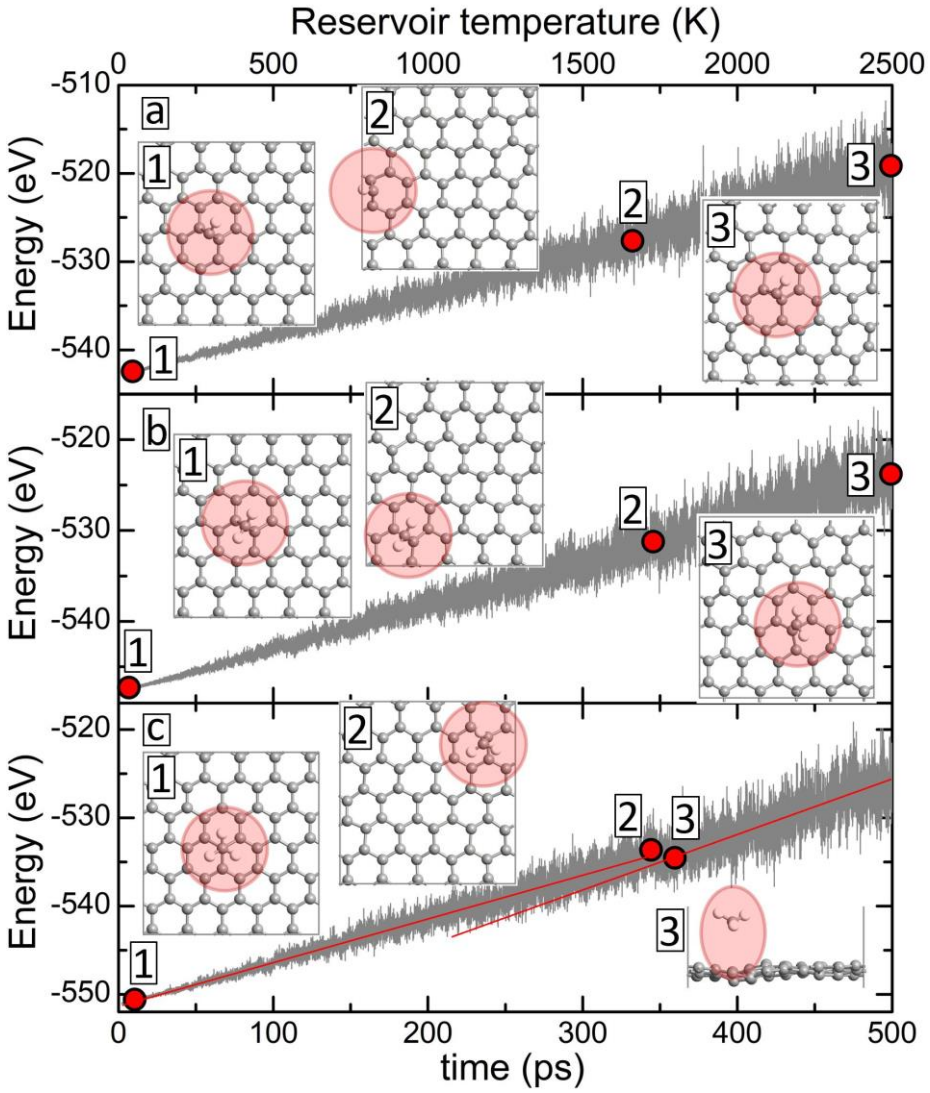

FIG. 4: Variations of potential energies of pristine graphene as functions of time (bottom axis) and reservoir temperature (top axis) for adsorbed CH (a), CH_2 (b) and CH_3 (c) plasma radicals. Insets show the structures at the time intervals indicated on the potential energy curve.

Next, we study the dynamics of the plasma particles on a graphene sheet with a single vacancy defect. Figure 5 shows the potential energy variations of graphene with a single vacancy defect as functions of time and reservoir temperature for all three plasma radicals.

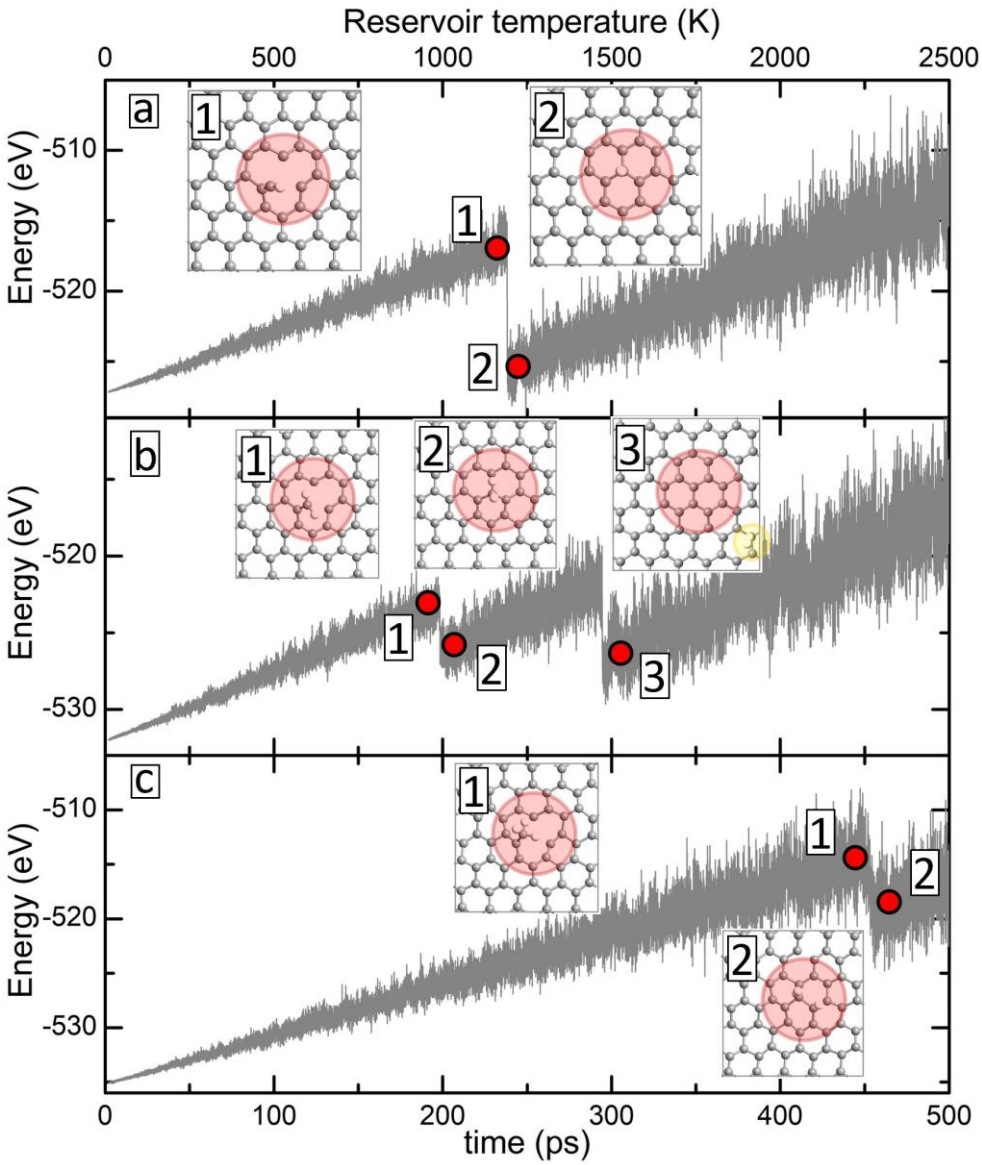

FIG. 5: Potential energy variations as functions of time (bot- tom axis) and reservoir temperature (top axis) when the plasma particles (CH (a), CH_2 (b) and CH_3 (c)) are adsorbed near a single vacancy defect. Insets show the snapshots of the system before (insets 1) and after (insets 2 and 3) graphene healing.

Notice that we start out MD simulations from the initial structures when the plasma particles are adsorbed near the edge of the defect (see all insets 1 in Fig. 5). If they are adsorbed away from the defected areas, they can diffuse over graphene (see supplemental online videos 1-3) and get pinned near the vacancy defect [39]. For the CH particle, a structural change occurs at 1190 K characterized by a sharp drop in the potential curve (see Fig. 5 (a)). As shown in inset 2 of Fig. 5 (a), this transition corresponds to the healing of the vacancy defect by the carbon atom of the CH radical. Healing of the vacancy defect is also obtained for the other plasma radicals with clear changes in the potential energy curves (see Figs. 5 and (c)). The healing mechanism

for CH_2 particle turns out to be slightly complex: two consecutive jumps are obtained in the potential energy in this case, corresponding to bond formation between the carbon atom of the plasma radical and the neighboring carbon atom of graphene (inset 2 in Fig. 5 (b)) and complete healing of the graphene and desorption of both hydrogen atoms as a molecule (inset 3 in Fig. 5 (b)). In the case of the CH_3 particle, hydrogen atoms diffuse to the neighboring carbon atoms of the graphene, followed by patching the vacancy defect by the carbon atom of the plasma particle (see inset 2 in Fig. 5 (c)). Notice that hydrogen atoms are still adsorbed on the graphene. It is known that hydrogen atoms are weakly adsorbed on the surface of graphene and they can be desorbed even at room temperature for a sufficiently long time [40]. However, it is computationally very demanding to conduct simulations for such long time periods even using force-field calculations. It should be mentioned that, in the CH_3 case, two hydrogen atoms bound to the same carbon atom are eventually desorbed from the surface as a molecule (similar to the CH_2 case). Consequently, a single hydrogen atom remains on the graphene surface (similar to the CH case). Hence, the healing of the vacancy defect by CH_x radicals containing odd numbers of H atoms results in a hydrogenated graphene surface, whereas the radicals containing even numbers of H atoms lead to a pristine graphene surface. Thus, the simulation results show the possibility of healing the vacancy defects in graphene using hydrocarbon plasma radicals.

One clear feature of the potential energy curves presented in Fig.5 is that the threshold point of the healing temperature increases with increasing the hydrogen content in the plasma particles. Correctly estimate the threshold temperature, a canonical (NVT) ensemble is applied in MD simulations using the Berendsen thermostat with a damping constant of 100 fs for 500 ps. Figures 6 (a) and (b) shows the potential energy variations as a function of time for CH_3 particle at temperatures 1800 K and 2000 K, respectively. It is obvious that the healing processes take place at smaller time intervals with increasing temperature (see Fig. 6 (a, b)). Notice also that the value of the threshold temperature is smaller than the one obtained during the simulations with temperature ramp (see Fig. 5 (c)). This phenomenon can probably be explained by the formation of internal pressure (or stress) in the simulation system, which affects the activation energy barrier of the defect-healing reaction [52].

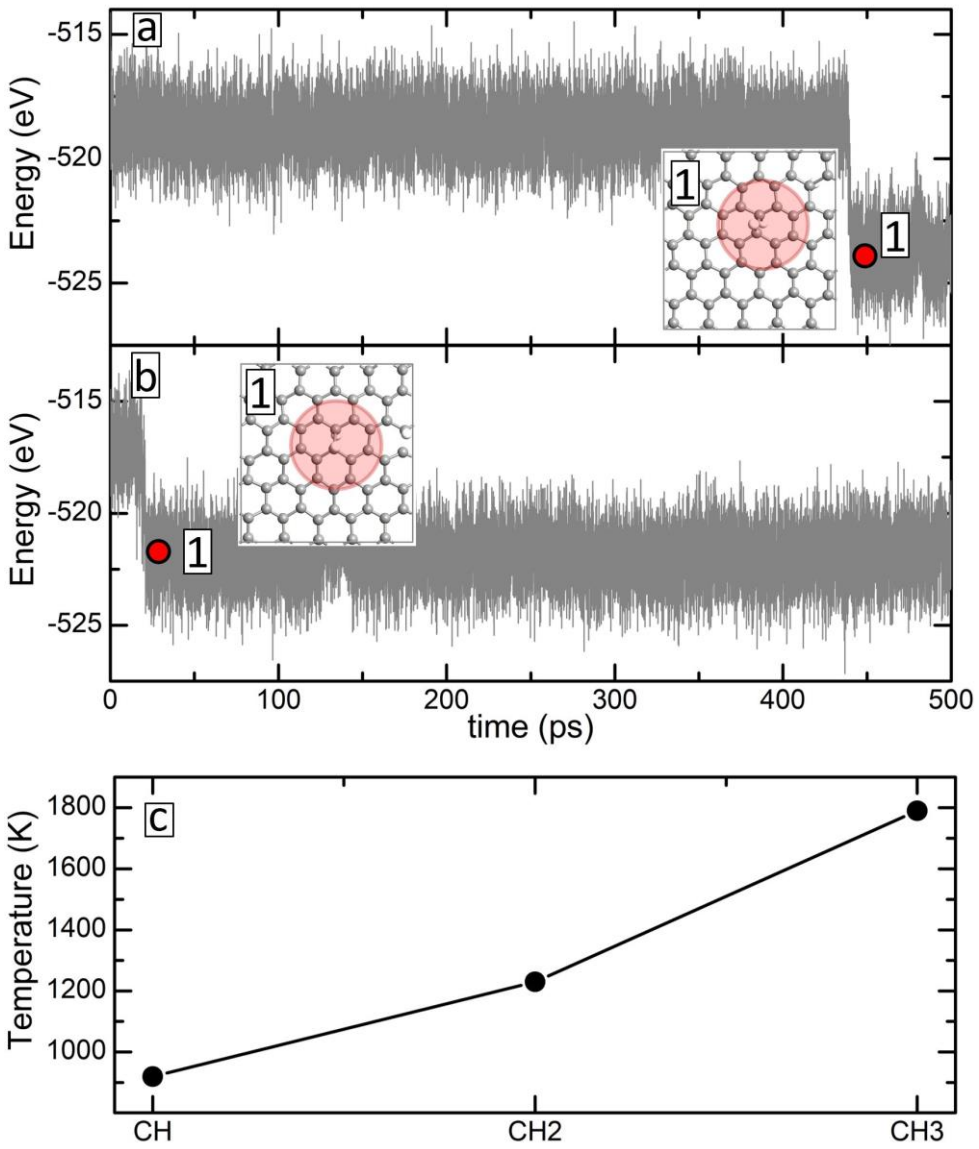

FIG. 6: (a, b) Potential energy variations as a function of time for a single vacancy defect with adsorbed CH_3 radical at temperatures 1800 K (a) and 2000 K (b). Insets show the structures of healed graphene at time intervals indicated on the potential energy curves. (c) The threshold temperature required to heal the single vacancy defect of graphene during 500 ps MD simulations at constant temperatures.

Figure 6 (c) summarizes our findings where we show the threshold point of the healing temperature for the single vacancy defect in graphene using the three plasma radicals. The threshold temperature values are obtained by averaging the temperatures over 4 different simulation runs for the given radicals. As is clear, the healing process occurs at relatively high temperatures and the threshold temperature increases almost linearly with increasing the hydrogen content in the plasma radicals. However, the MD calculations are conducted at higher temperatures to obtain chemical reactions within a short time scale (in the picoseconds range). Therefore, we expect smaller threshold temperatures in real experiments. Despite a larger

threshold healing temperature, the CH_3 radical can be considered the best particle for the healing of vacancy defects in graphene compared to the other two plasma radicals. Namely, it disturbs graphene's planar structure insignificantly (see insets 3 and 6 in Fig. 1 (a)) and can be desorbed from the non-defects regions of graphene at relatively smaller temperatures (see inset 2 in Fig. 4 (c)) due to smaller adsorption energy (see Fig. 1).

We have also studied the possibility of plasma healing of divacancy defect in graphene, which is one of the most abundant and important defects affecting the properties of the material [53]. As an example, we present in Fig. 7 the variations of the potential energy of the graphene sheet with a divacancy defect in the presence of two CH plasma radicals as a function of time/temperature.

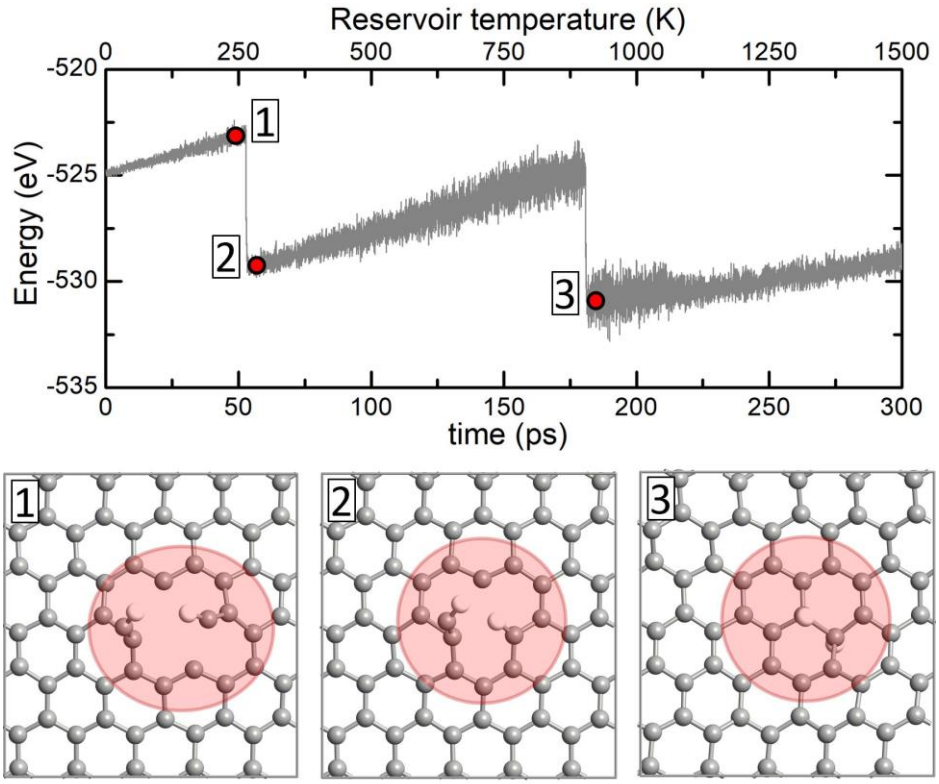

FIG. 7: Potential energy variations as functions of time (bottom axis) and reservoir temperature (top axis) when two CH plasma radicals are adsorbed near divacancy defect. Panels 1-3 show the snapshots of the system before (insets 1) and after (insets 2 and 3) graphene healing as indicated on the potential energy curve.

Both of the plasma particles are adsorbed at the edges of the defect (see panel 1). The first sharp drop on the potential energy curve corresponds to the state where the carbon atom of one of the CH particles takes the place of the missing carbon atom of graphene (panel 2). After the second potential energy drop, the planar structure of graphene gets restored with complete healing of the divacancy defect (panel 3). Thus, plasma treatment can also heal the larger size vacancy

defects.

Finally, we study the effect of the plasma particles on the heat treatment of the Stone-Wales defect, which is created by the rotation of the carbon-carbon bond. This defect is characterized by a very high restoration energy barrier (~6 eV [31]) which can be reduced by the adsorption of either transition metal atoms (2.86 eV) [54] or carbon adatom (0.86 eV) [55]. Figure 8 shows the variations of the potential energy of the graphene sheet with a Stone-Wales defect as a function of time/temperature in the presence of CH (a) and CH_2 (b) plasma radicals.

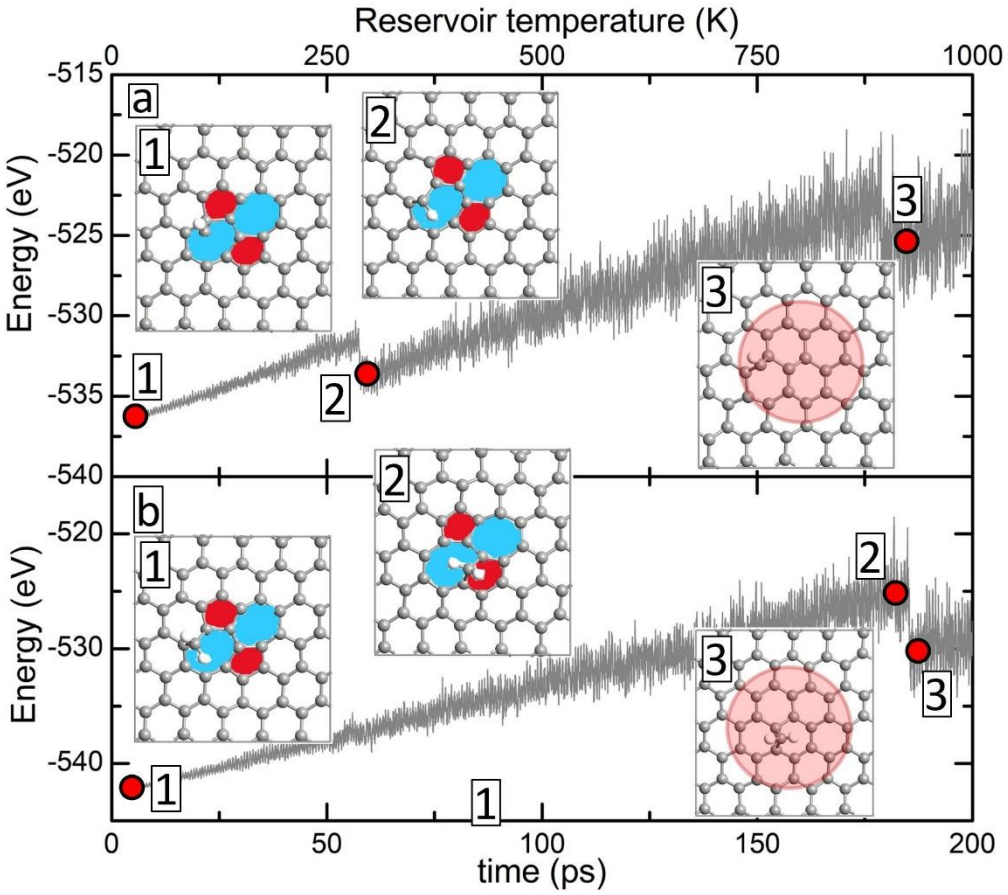

FIG. 8: Potential energy variations as functions of time (bottom axis) and reservoir temperature (top axis) when the plasma particles CH (a) and CH_2 (b) are initially adsorbed near Stone-Wales defects. Insets show the snapshots of the system before (insets 1 and 2) and after (insets 3) the healing.

Initially, the plasma particles are adsorbed at the edge of the heptagonal ring (see panels 1 in Figs. 8 (a, b)), which are the ground state configurations. With increasing temperature, the CH plasma particle transits from T-site adsorption (panel 1 in Fig. 8 (a)) to bridge site adsorption with a small drop on the potential energy curve. With further increasing temperature, the Stone-Wales defect gets healed and the hexagonal structure of graphene is restored (see panel 3 in

Fig. 8 (a)). The CH_2 particle is also initially adsorbed on the heptagonal rings (panel 1 in Fig. 8 (b)), which turns out to be mobile at larger temperatures (panel 2 in Fig. 8 (b)). This plasma particle also triggers the restoration of the hexagonal structure of graphene as shown in panel 3 of Fig. 8 (b). Thus, the plasma treatment can also be used for the healing of the Stone-Wales defects in graphene.

VI. CONCLUSIONS

DFT-based NEB calculations and reactive molecular dynamics simulations are conducted to study the possibility of healing the vacancy defects in graphene using methane plasma radicals CH_x (x=1-3). At high temperatures, the carbon atom of the plasma particles substitutes the missing carbon atom and produces the reconstruction of the perfect hexagonal structure of graphene. This process takes place at different temperatures and with different mechanisms depending on the hydrogen content of the plasma particle. Meanwhile, no imperfections are created in pristine graphene due to the adsorption of the plasma particles. Plasma-assisted healing of Stone-Wales defects is also obtained, which is one of the important structural defects in carbon-based materials with very high restoration energy. These findings can be useful for practical applications in healing structural defects in graphene using methane-based plasma particles with no further damage to the hexagonal graphene framework.

ACKNOWLEDGEMENTS

U.K. and M.Y. acknowledge the support of Agency for Innovative Development, Uzbekistan (Grant number: F-FA-2021-512). G.B.E. acknowledges support from the Ministry of Higher Education, Science and Innovations (Grant number: FZ-2020092435). The computational resources and services used in this work were partially provided by the HPC core facility CalcUA of the Universiteit Antwerpen and VSC (Flemish Supercomputer Center), funded by the FWO and the Flemish Government.

REFERENCES

1. A. K. Geim, Graphene: Status and Prospects, Science 324 (2009) 1530-1534.
2. C. Neto, F. Guinea, N. M. R. Peres, K. S. Novoselov, and K. Geim, The electronic properties of graphene, Rev. Mod. Phys. 81 (2009) 109.
3. K. S. Novoselov, A. K. Geim, S. V. Morozov, D. Jiang, Y. Zhang, S. V. Dubonos, I. V. Grigorieva, and A. A. Firsov, Electric Field Effect in Atomically Thin Carbon Films, Science 306 (2004) 666-669.
4. A. K. Geim and K. S. Novoselov, The rise of graphene, Nat. Mater. 6 (2007) 183-191.
5. M. H. Gass, U. Bangert, A. L. Bleloch, P. Wan, R. R. Nair, and A. K. Geim, Free-standing graphene at atomic resolution, Nature Nanotechnology 3 (2008) 676-681.
6. J. C. Meyer, C. Kisielowski, R. Erni, M. D. Rossell, M.F. Crommie, and A. Zettl, Direct Imaging of Lattice Atomsand Topological Defects in Graphene Membranes, Nano Lett. 8 (2008) 3582-3586.
7. A. Eckmann, A. Felten, A. Mishchenko, L. Britnell, R. Krupke, K. S. Novoselov, and C. Casiraghi, Probing the Nature of Defects in Graphene by Raman Spectroscopy, Nano Lett. 12 (2012) 3925-3930.
8. F. Banhart, J. Kotakoski, and A. V. Krasheninnikov, Structural Defects in Graphene, ACS Nano 5 (2011) 26-41.
9. R. H. Telling and M. I. Heggie, Radiation defects in graphite, Philos. Mag. 87 (2007) 4797-4846.
10. X. Wang, S. M. Tabakman, and H. Dai, Atomic Layer Deposition of Metal Oxides on Pristine and Functionalized Graphene, J. Am. Chem. Soc. 130 (2008) 8152.
11. S. Malola, H. Hakkinen, and P. Koskinen, Gold in graphene: in-plane adsorption and diffusion, Appl. Phys. Lett. 94 (2009) 043106.
12. A. V. Krasheninnikov, P. O. Lehtinen, A. S. Foster, P. Pyykko, and R. M. Nieminen, Embedding Transition-Metal Atoms in Graphene: Structure, Bonding, and Magnetism, Phys. Rev. Lett. 102 (2009) 126807.
13. P. A. Denis, Density Functional Investigation of Thioepoxidated and Thiolated Graphene, J. Phys. Chem. C 113 (2009) 5612-5619.
14. N. Ghaderi and M. Peressi, First-Principle Study of Hydroxyl Functional Groups on Pristine, Defected Graphene, and Graphene Epoxide, J. Phys. Chem. C 114 (2010) 21625-21625.
15. R. Zan, Q. Ramasse, U. Bangert, and K. Novoselov, Graphene reknits its holes, Nano Lett. 12 (8) (2012) 3936-3940.
16. B. Song, G.F. Schneider, Q. Xu, G. Pandraud, C. Dekker, and H. Zandbergen, Atomic-scale electron-beam sculpt- ing of near-defect-free graphene nanostructures, Nano Lett. 11 (6) (2011) 2247-2250.
17. J. Chen, T. Shi, T. Cai, T. Xu, L. Sun, X. Wu, and D. Yu, Self healing of defected graphene, Appl. Phys. Lett. 102 (2013) 103107.
18. K. K. H. De Silva, H.-H. Huang, R. Joshi, and M. Yoshimura, Restoration of the graphitic structure by defect repair during the thermal reduction of graphene oxide, Carbon N. Y. 166 (2020) 74-90.
19. I. N. Kholmanov, J. Edgeworth, E. Cavaliere, L. Gavioli, Magnuson, and R. S. Ruoff, Healing of structural defects in the topmost layer of graphite by chemical vapor deposition, Adv. Mater. 23 (2011) 1675-1678.
20. L. Wang and F. Duan, Healing mechanism of multi-vacancy defective graphene under carbon irradiation, Fullerenes, nanotubes and carbon nanostructures 27 (2019) 247-255.
21. T. Botari, R. Paupitz, P. A. da Silva Autreto, and D. S. Galvao, Graphene healing mechanisms: A theoretical investigation, Carbon 99 (2016) 302-309.
22. L. Kong, X. Wang, W. Zheng, S. Tian, Y. Qi, Y. Xue, and B. Wang, Effects of plasma treatment on properties

of carbon fiber and its reinforced resin composites, Mater. Res. Express 7 (2020) 065304.

23. G. Lota, J. Tyczkowski, R. Kapica, K. Lota, and E. Frackowiak, Carbon materials modified by plasma treatment as electrodes for supercapacitors, J. Power Sources 195 (2010) 7535-7539.
24. C. Saka, Overview on the Surface Functionalization Mechanism and Determination of Surface Functional Groups of Plasma Treated Carbon Nanotubes, Crit. Rev. Anal. Chem. 48 (2018) 1-14.
25. R. J. Zaldivar, J.P. Nokes, P.M. Adams, K. Hammoud, H.I. Kim, Surface functionalization without lattice degradation of highly crystalline nanoscaled carbon materials using a carbon monoxide atmospheric plasma treatment, Carbon 50 (2012) 2966-2975.
26. M. Chen, H. Zhou, C. Qiu, H. Yang, F. Yu, and L. Sun, Layer-dependent fluorination and doping of graphene via plasma treatment, Nanotechnology 23 (2012) 115706.
27. N. McEvoy, H. Nolan, N. A. Kumar, T. Hallam, and G. S. Duesberg, Functionalisation of graphene surfaces with downstream plasma treatments, Carbon 54 (2013) 283-290.
28. W. Yue, C. H. Ra, X. C. Liu, D. Y. Lee, and W. J. Yoo, Edge contacts of graphene formed by using a controlled plasma treatment, Nanoscale, 7 (2015) 825-831.
29. M. Rybin, A. Pereyaslavtsev, T. Vasilieva, V. Myasnikov, I. Sokolov, A. Pavlova, E. Obraztsova, Khomich, V. Ralchenko, and E. Obraztsova, Efficient nitrogen doping of graphene by plasma treatment, Carbon 96 (2016) 196-202.
30. A. J. Stone and D. J. Wales, Theoretical studies of icosahedral C60 and some related species, Chem. Phys. Lett. 128 (1986) 501-503.
31. M D. Bhatt, H. Kim, and G. Kim, Various defects in graphene: a review, RSC Adv. 12 (2022) 21520-21547.
32. A. C. T. van Duin, S. Dasgupta, F. Lorant, and W. A. Goddard, ReaxFF: A Reactive Force Field for Hydrocarbons, J. Phys. Chem. A 105 (2001) 9396-9409.
33. U. Khalilov, A. Bogaerts, and E. C. Neyts, Microscopic mechanisms of vertical graphene and carbon nanotube cap nucleation from hydrocarbon growth precursors, Nanoscale 6 (2014) 9206-9214.
34. G. R. Berdiyorov, M. Neek-Amal, F. M. Peeters, and C. T. Van Duin, Stabilized silicene within bilayer graphene: A proposal based on molecular dynamics and density-functional tight-binding calculations, Physical Review B 89 (2014) 024107.
35. U. Khalilov, A. Bogaerts, and E. C. Neyts, Atomic scale simulation of carbon nanotube nucleation from hydrocarbon precursors, Nat. Commun. 6 (2015) 10306.
36. A. Sadeghi, M. Neek-Amal, G. R. Berdiyorov, and F. M. Peeters, Diffusion of fluorine on and between graphene layers, Physical Review B 91 (2015) 014304.
37. G. R. Berdiyorov, B. Mortazavi, S. Ahzi, F. M. Peeters, and M. K. Khraisheh, Effect of straining graphene on nanopore creation using Si cluster bombardment: A re- active atomistic investigation, Journal of Applied Physics 120 (2016) 225108.
38. U. Khalilov, C. Vets, and E. C. Neyts, Molecular evidence for feedstock-dependent nucleation mechanisms of CNTs, Nanoscale Horiz. 4 (2019) 674-682.
39. G. R. Berdiyorov, M. V. Milosevic, F. M. Peeters, A. C. T. Van Duin, Stability of CH_3 molecules trapped on hydrogenated sites of graphene, Physica B 455 (2014) 60-65.
40. R. Erni, M. D. Rossell, M.-T. Nguyen, S. Blankenburg, D. Passerone, P. Hartel, N. Alem, K. Erickson, W. Gannett, and A. Zettl, Stability and dynamics of small molecules trapped on graphene, Phys. Rev. B 82 (2010) 165443.
41. M. Shariat, S. Hosseini, B. Shokri, and E. Neyts, Plasma enhanced growth of single walled carbon nanotubes at

low temperature: a reactive molecular dynamics simulation, Carbon 65 (2013) 269-276.

42. U. Khalilov, A. Bogaerts, S. Hussain, E. Kovacevic, P. Brault, C. Boulmer-Leborgne, and E. C. Neyts, Nanoscale mechanisms of CNT growth and etching in plasma environment, J. Phys. D: Appl. Phys. 50 (2017) 184001.
43. J. P. Perdew, K. Burke, M. Ernzerhof, Generalized Gradient Approximation Made Simple, Phys. Rev. Lett. 77 (1996) 3865.
44. S. Grimme, Semiempirical GGA-type density functional constructed with a long-range dispersion correction, J. Comp. Chem. 27 (2006) 1787-1799.
45. H. J. Monkhorst and J. D. Pack, Special points for Brillouin-zone integrations, Phys. Rev. B 13 (1976) 5188.
46. G. Henkelman and H. Jonsson, A climbing image nudged elastic band method for finding saddle points and minimum energy paths, J. Chem. Phys 113 (2000) 9901-9978.
47. V. Asgeirsson, B. O. Birgisson, R. Bjornsson, U. Becker, F. Neese, C. Riplinger, and H. Jonsson, Nudged Elastic Band Method for Molecular Re- actions Using Energy-Weighted Springs Combined with Eigenvector Following, J. Chem. Theory Comput. 17 (2021) 4929-4945.
48. G. R. Berdiyorov, E. Elbashier, G. Carchini, I.A. Hussein, and A. Sakhaee-Pour, The effect of vacancy defects on the adsorption of methane on calcite 104 surface, J. Mater. Sci. Technol. 14 (2021) 3051-3058.
49. S. Smidstrup, D. Stradi, J. Wellendorff, P. A. Khomyakov, U. G. Vej-Hansen, M-E. Lee, T. Ghosh, E. Jonsson, H. Jonsson, and K. Stokbro, First-principles Green's-function method for surface calculations: A pseudopotential localized basis set approach, Phys. Rev. B 96 (2017) 195309.
50. S. Smidstrup, T. Markussen, P. Vancraeyveld, J. Wellendorff, J. Schneider, T. Gunst, B. Verstichel, D. Stradi, P. Khomyakov, and U. G Vej-Hansen, QuantumATK: An integrated platform of electronic and atomic-scale modelling tools, J. Phys.: Condens. Matter 32 (2020) 015901.
51. H. Berendsen, J. P. M. Postma, W. van Gunsteren, A. DiNola, and J. R. Haak, Molecular-Dynamics with Coupling to An External Bath, The Journal of Chemical Physics 81 (1984) 3684.
52. U. Khalilov, A. Bogaerts, and E. C. Neyts, Toward the Understanding of Selective Si Nano-Oxidation by Atomic Scale Simulations, Acc. Chem. Res. 50 (2017) 796-804.
53. C. O. Girit, J. C. Meyer, R. Erni, M. D. Rossell, Kisielowski, L. Yang, C,-H. Park, M. F. Crommie, M. L. Cohen, S. G. Louie, and A. Zettl, Graphene at the Edge: Stability and Dynamics, Science 323 (2009) 1705-1708.
54. W. W. Wang, J. S. Dang, J. J. Zheng, X. Zhao, E. Osawa and S. Nagase, Metal-promoted restoration of defective graphene, J. Mater. Chem. 22 (2012) 16370-16375.
55. C. Wang and Y.-H. Ding, Catalytically healing the Stone-Wales defects in graphene by carbon adatoms, J. Mater. Chem. A 1 (2013) 1885-1891.